



## UWS Academic Portal

### Asymptotic properties of radial A+BC reaction fronts

Trevelyan, Philip; Walker, Alan

*Published in:*  
Physical Review E

*DOI:*  
[10.1103/PhysRevE.98.032118](https://doi.org/10.1103/PhysRevE.98.032118)

Published: 13/09/2018

*Document Version*  
Peer reviewed version

[Link to publication on the UWS Academic Portal](#)

*Citation for published version (APA):*

Trevelyan, P., & Walker, A. (2018). Asymptotic properties of radial A+BC reaction fronts. *Physical Review E*, 98, [032118]. <https://doi.org/10.1103/PhysRevE.98.032118>

#### General rights

Copyright and moral rights for the publications made accessible in the UWS Academic Portal are retained by the authors and/or other copyright owners and it is a condition of accessing publications that users recognise and abide by the legal requirements associated with these rights.

#### Take down policy

If you believe that this document breaches copyright please contact [pure@uws.ac.uk](mailto:pure@uws.ac.uk) providing details, and we will remove access to the work immediately and investigate your claim.

# Asymptotic properties of radial $A+B\rightarrow C$ reaction fronts

P. M. J. Trevelyan

*Faculty of Computing, Engineering and Science, University of South Wales, Pontypridd, CF37 1DL, United Kingdom*

A. J. Walker

*School of Computing, Engineering and Physical Sciences,  
University of the West of Scotland, Paisley, PA1 2BE, United Kingdom*

(Dated: August 13, 2018)

If two initially separated solutions of reactants are put in contact and a simple  $A + B \rightarrow C$  reaction takes place, reaction-diffusion profiles develop due to the coupling of reaction and diffusion. The properties of such fronts are well known in the case of an initially planar contact line between the two solutions. In this study one of the reactants is injected at a constant flux from a point source into a miscible solution of the other reactant so that the reaction front expands out radially. Both the leading order large time and small time asymptotic limits of the reactant concentrations and reaction front position are obtained analytically. Just as in the planar reaction front case, the position of the reaction front scales like  $t^{1/2}$  and the width of the reaction front scales with  $t^{1/6}$ . In the large Péclet number limit the large time asymptotic properties of the radial reaction front are found to be similar to those of the planar front except that the profiles are advected with the fluid flow. The distance between the contact line and the position of the radial reaction front is  $1/\sqrt{2}$  of the distance that a planar reaction front travels. Further, the length scales inside and outside of the reaction zone are reduced by factors of  $2^{1/6}$  and  $\sqrt{2}$ , respectively, compared to the planar reaction front.

PACS numbers: 82.20.Db, 82.20.Wt, 82.40.-g

## I. INTRODUCTION

The behaviour of many chemical systems is determined by the evolution of a reaction front formed between initially separated reactants [1, 2]. The simplest model of this phenomenon consists of two species  $A$  and  $B$  mixing and reacting at time  $t = 0$  to form a reaction front producing species  $C$  ( $A + B \rightarrow C$ ). When the chemical reaction changes a fluid's physical properties (density, viscosity, etc.) then convection can be induced. Experiments portraying these changes have often focused on Hele-Shaw cells [3–6].

A Hele-Shaw cell is a quasi-2D geometrical cell formed from two glass plates in which the reactive solutions are contained. One acidic solution is placed on top of another, more dense, miscible solution containing a reactant. Convective instabilities occur from double diffusive instabilities or changes in the density profile induced by chemical reaction and diffusion.

Theory and experiments on convection induced by chemical reactions have analysed various instabilities that can deform reaction-diffusion base states [3, 7–11]. Furthermore, there exist many articles considering the small and large time asymptotic properties of these reaction fronts in the case where the two initially separated reactants are brought into contact along a planar interface. For large times  $T$ , Venzl [12] showed that the position of the reaction front scales with  $T^{1/2}$  when the reactants have equal diffusion coefficients. Gálfi and Rácz [13] found that the reaction zone width scaled with  $T^{1/6}$  and the rate of production at the reaction front scaled with  $T^{-2/3}$ . The results by Gálfi and Rácz were found

to be in good agreement with results from experiments conducted in gels [14, 15]. These results were generalised by Koza [16] for non-equal diffusion coefficients. Sinder and Pelleg were then able to obtain the solution for the product  $C$  [17]. Cornell *et al.* [18–20] were able to prove similar results for the reaction front and rate using the reaction  $nA + mB \rightarrow C$ . The properties of this reaction front were investigated further by Trevelyan [21, 22]. It was found that reaction fronts could travel with different time scalings when the reactants diffuse at different rates and the initial concentration ratio is chosen appropriately.

The small time asymptotic properties of the reaction  $A + B \rightarrow C$  are discussed by Trevelyan [22]. It can be said that these properties are not as clearly understood as the large time counterparts. Nevertheless, Taitelbaum *et al.* found that the position and width of the reaction front and the total rate of production were found to scale with  $T^{1/2}$  for small times [23]. Furthermore, the first-order correction to the solution was analytically expressed in terms of a double integral using the Green function for the diffusion equation. The correction to the total rate of the reaction was found to scale with  $T^{3/2}$ . Taitelbaum *et al.* also introduced approximate solutions for the small-time limit and found that the reaction front could change direction under certain conditions upon the initial concentration ratio and the ratio of the diffusion coefficients [24]. Similar approximate solutions have been found by Hecht and Taitelbaum [25]. A double-direction change was numerically found by Taitelbaum and Koza [26].

However, the bulk of the aforementioned research has focused on modeling and analysing the reactive inter-

face between chemicals  $A$  and  $B$  on a line or Cartesian plane. This is not an appropriate coordinate system for experiments where one wishes to inject one chemical into another, which corresponds to a single point source. Clearly, the use of a polar coordinate system for these cases is required. Brau *et al.* studied the dynamics of  $A + B \rightarrow C$  fronts by radial injection, computing the long-time evolution of the front position, its width, and production rates of the product [27]. Their work compared well with calcium carbonate precipitation experiments [28].

In this article, we consider both the small- and large-time asymptotic solutions in the case of a constant flux from a point source. Furthermore, we investigate the concentration profiles of the reaction fronts in these limits for both slow and fast flow rates. Analytical results are presented, alongside both small- and large-time asymptotics in the special case of equal diffusion coefficients. A mathematical model of the Hele-Shaw cell is presented in section II, with the corresponding numerical solutions provided in section III. The small- and large-time asymptotic (outer and inner) solutions are discussed in section IV, V and VI respectively. Finally, the results are discussed in section VII.

## II. MODEL

Consider a Hele-Shaw cell initially filled with a solution containing a reactant  $B$  at concentration  $B_0$ . At time  $T = 0$  a solution containing reactant  $A$  at concentration  $A_0$  is injected into the centre of the Hele-Shaw cell through a point source. If no instabilities are present then the solution containing reactant  $A$  will spread out radially.

Upon contact, the two species react via the bimolecular reaction



generating a product  $C$ .

The gap width  $h$ , of the Hele-Shaw cell is assumed to be sufficiently small so that Darcy's law can be utilized and the domain can be considered as two-dimensional. The reactive solutions are considered sufficiently dilute so that saturation effects can be ignored and that the diffusion coefficients can be considered as constants. The resulting two-dimensional equations describing the dynamics of such a system are the following:

$$\begin{aligned} \nabla P &= -\frac{M}{K} \underline{U} \\ \nabla \cdot \underline{U} &= 0 \\ \frac{\partial A}{\partial T} + \underline{U} \cdot \nabla A &= D_A \nabla^2 A - kAB \\ \frac{\partial B}{\partial T} + \underline{U} \cdot \nabla B &= D_B \nabla^2 B - kAB \\ \frac{\partial C}{\partial T} + \underline{U} \cdot \nabla C &= D_C \nabla^2 C + kAB \end{aligned}$$

where  $A$ ,  $B$  and  $C$  denote the concentration of their respective species,  $P$  is the pressure,  $\underline{U}$  is the velocity,  $M$  is the dynamic viscosity,  $K = h^2/12$  is the permeability of the Hele-Shaw cell,  $k$  is the kinetic constant of the reaction,  $D_A$ ,  $D_B$ ,  $D_C$  are the molecular diffusion coefficients of species  $A$ ,  $B$  and  $C$ , respectively.

As we consider a radial injection, the equations are written in polar coordinates  $(R, \theta)$  for which  $\nabla = (\frac{\partial}{\partial R}, \frac{1}{R} \frac{\partial}{\partial \theta})$  and  $\nabla^2 = \frac{1}{R} \frac{\partial}{\partial R} (R \frac{\partial}{\partial R}) + \frac{1}{R^2} \frac{\partial^2}{\partial \theta^2}$ . The velocity is expressed as  $\underline{U} = (U_R, U_\theta)$  to denote the radial and angular velocity components.

We introduce the following nondimensionalization:

$$\begin{aligned} t &= T/T_0, \quad r = R/L_0, \quad (u, v) = (U_R, U_\theta)/U_0 \\ (a, b, c) &= (A, B, C)/A_0, \quad \mu = M/\mu_0, \quad p = P/P_0. \end{aligned}$$

Hence we define  $P_0 = \mu_0 D_A / K$ ,  $T_0 = 1/(kA_0)$ ,  $L_0 = \sqrt{D_A/(kA_0)}$  and  $U_0 = \sqrt{kA_0 D_A}$ . Further, we define  $\delta_b = D_A/D_B$  and  $\delta_c = D_A/D_C$  to yield the equations

$$p_r = -\mu u \quad (2a)$$

$$\frac{1}{r} p_\theta = -\mu v \quad (2b)$$

$$(ru)_r + v_\theta = 0 \quad (2c)$$

$$a_t + ua_r + \frac{v}{r} a_\theta = \frac{1}{r} (ra_r)_r + \frac{a_{\theta\theta}}{r^2} - ab \quad (2d)$$

$$b_t + ub_r + \frac{v}{r} b_\theta = \frac{1}{\delta_b} \left[ \frac{1}{r} (rb_r)_r + \frac{b_{\theta\theta}}{r^2} \right] - ab \quad (2e)$$

$$c_t + uc_r + \frac{v}{r} c_\theta = \frac{1}{\delta_c} \left[ \frac{1}{r} (rc_r)_r + \frac{c_{\theta\theta}}{r^2} \right] + ab. \quad (2f)$$

In the absence of an instability of the front we can assume the problem is independent of  $\theta$  with  $v = 0$ . Hence the flow equation depends only on the 1D radial direction, so the pressure and velocity satisfy

$$\begin{aligned} p_r &= -\mu u \\ (ru)_r &= 0. \end{aligned}$$

Thus  $u$  is inversely proportional to  $r$  and we write the solution as

$$u = \frac{2\text{Pe}}{r} \quad (3)$$

where,  $u$  and  $p$  are undefined at  $r = 0$ , and at this stage,  $\text{Pe}$  is an integration constant. If  $\mu$  is a constant then  $p = -2\text{Pe}\mu \ln(r)$ .

The constant  $\text{Pe}$  can be determined by noting that the flux  $Q$  of the injected fluid is given by

$$\begin{aligned} Q &= \int_0^{2\pi} \underline{U} \cdot \underline{e}_r R d\theta = \int_0^{2\pi} U_R R d\theta = \int_0^{2\pi} U_0 L_0 u r d\theta \\ &= \int_0^{2\pi} 2U_0 L_0 \text{Pe} d\theta = 4\pi U_0 L_0 \text{Pe} = 4\pi D_A \text{Pe} \end{aligned}$$

where  $\underline{e}_r$  is the unit vector in the radial direction. Hence, in this problem we identify  $\text{Pe}$  as the Péclet number of

the problem and is defined as

$$\text{Pe} = \frac{Q}{4\pi D_A} \quad (4)$$

which measures the balance between advection and diffusion.

In the absence of diffusion, the contact line between the two liquids is an expanding circle and so the position of the contact line can be fully described by the radius of the expanding circle. Let  $r_c$  denote the position of the moving contact line. The contact line moves at the same speed as the velocity. As the fluid velocity  $u$  is given by equation (3), therefore  $\frac{d}{dt}r_c = u = 2\text{Pe}/r_c$  at  $r = r_c$ . Thus  $\frac{d}{dt}r_c^2 = 4\text{Pe}$ , and so  $r_c^2 = 4\text{Pe}t$  as  $r_c = 0$  at  $t = 0$ . Hence, we have obtained

$$r_c = 2\sqrt{\text{Pe}t}, \quad (5)$$

the position of the moving contact line. In dimensional variables, the position of the contact line is given by  $R_c = 2\sqrt{\text{Pe}D_A T} = \sqrt{QT/\pi}$ .

Substituting the solution (3) for  $u$  into the system of equations (2) yields

$$a_t + (2\text{Pe} - 1)\frac{a_r}{r} = a_{rr} - ab \quad (6a)$$

$$b_t + \left(2\text{Pe} - \frac{1}{\delta_b}\right)\frac{b_r}{r} = \frac{b_{rr}}{\delta_b} - ab \quad (6b)$$

$$c_t + \left(2\text{Pe} - \frac{1}{\delta_c}\right)\frac{c_r}{r} = \frac{c_{rr}}{\delta_c} + ab \quad (6c)$$

These are the differential reaction-diffusion-advection equations that will be considered throughout the rest of the paper.

Initially the Hele-Shaw cell only contains reactant B and so, at  $t = 0$ , we have the initial condition

$$b = \varphi, \quad a = c = 0 \quad \text{for } r \neq 0$$

where  $\varphi = B_0/A_0$ . At  $r = 0$ , a solution containing reactant A is being injected into the Hele-Shaw cell, therefore the boundary condition at the injection point is

$$a = 1, \quad b = c = 0 \quad \text{at } r = 0.$$

The far field boundary condition is given by

$$a \rightarrow 0, \quad b \rightarrow \varphi, \quad c \rightarrow 0 \quad \text{as } r \rightarrow \infty.$$

Introducing

$$\eta = r/\sqrt{4t}$$

and  $\tau = t$  we next change from  $(r, t)$  coordinates to  $(\eta, \tau)$  coordinates which yields

$$\tau a_\tau - \frac{\eta}{2}a_\eta + (2\text{Pe} - 1)\frac{a_\eta}{4\eta} = \frac{a_{\eta\eta}}{4} - ab\tau \quad (7a)$$

$$\tau b_\tau - \frac{\eta}{2}b_\eta + \left(2\text{Pe} - \frac{1}{\delta_b}\right)\frac{b_\eta}{4\eta} = \frac{b_{\eta\eta}}{4\delta_b} - ab\tau \quad (7b)$$

$$\tau c_\tau - \frac{\eta}{2}c_\eta + \left(2\text{Pe} - \frac{1}{\delta_c}\right)\frac{c_\eta}{4\eta} = \frac{c_{\eta\eta}}{4\delta_c} + ab\tau \quad (7c)$$

The similarity variable  $\eta$  allows the initial conditions and the boundary conditions to be written together as

$$a = 1, \quad b = c = 0 \quad \text{at } \eta = 0 \quad (7d)$$

$$b \rightarrow \varphi, \quad a \rightarrow 0, \quad c \rightarrow 0 \quad \text{as } \eta \rightarrow \infty \quad (7e)$$

Equation (7) provide the system of equations that must be numerically solved to determine the solutions for  $a$ ,  $b$  and  $c$  in  $\eta$  and  $\tau$  coordinates. This problem depends on 4 parameters:  $\text{Pe}$ ,  $\varphi$ ,  $\delta_b$  and  $\delta_c$ . These parameters relate to the Péclet number ( $\text{Pe}$ ), the ratio of initial reactant concentrations ( $\varphi$ ), and the ratio of molecular diffusion coefficients ( $\delta_b$  and  $\delta_c$ ).

### III. NUMERICAL SOLUTIONS

Using a Crank-Nicolson method with finite differences we can numerically solve system (6). The typical small time evolution of the concentration profiles for  $a$ ,  $b$  and  $c$  for three values of  $\text{Pe}$  are illustrated in figure 1. In figure 1(a) the early stages of the slow flow regime are illustrated for  $\text{Pe}=0.1$ . We observe that species A and B have very sharp concentration gradients near  $r = 0$ . This is due to diffusion dominating over advection over the majority of the region, so that a boundary layer forms near  $r = 0$  where species A is being injected. In figure 1(b) the early stages of the moderate flow regime are illustrated for  $\text{Pe}=1$ . In this regime there are no boundary layers or sharp gradients as neither diffusion or advection is dominating. In figure 1(c) the early stages of the fast flow regime are illustrated for  $\text{Pe}=10$ . We observe that the concentration gradients of species A, B and C are all close to zero at  $r = 0$ . This is due to advection dominating over diffusion so that all of the species are by transported by the fluid flow.

The typical large time evolution of the concentration profiles for  $a$ ,  $b$  and  $c$  for three values of  $\text{Pe}$  are illustrated in figure 2. In figure 2(a) the late stages of the slow flow regime are illustrated for  $\text{Pe}=0.1$ . We observe that species A, B and C have sharp concentration gradients near  $\eta = 0$ . The maximum concentration of C approaches a constant and appears to move closer to  $\eta = 0$ , (although not illustrated, when plotted against  $r$  the local maximum in the concentration of C is found to move away from  $r = 0$  at the rate  $t^{1/6}$ .) This is due to the local maximum in C approaching the location of the maximum reaction rate in time. Similarly, the concentration gradient of A appears to get sharper in time near  $\eta = 0$ , although it is actually getting less steep in time. In figure 2(b) the late stages of the moderate flow regime are illustrated for  $\text{Pe}=1$ . In this regime both the reaction front and the maximum concentration of species C have moved away from  $\eta = 0$ . In figure 2(c) the late stages of the fast flow regime are illustrated for  $\text{Pe}=10$ . In this regime the reaction front has moved sufficiently far away from the point source that the concentration gradients of A, B and C each tend to zero away from the reaction

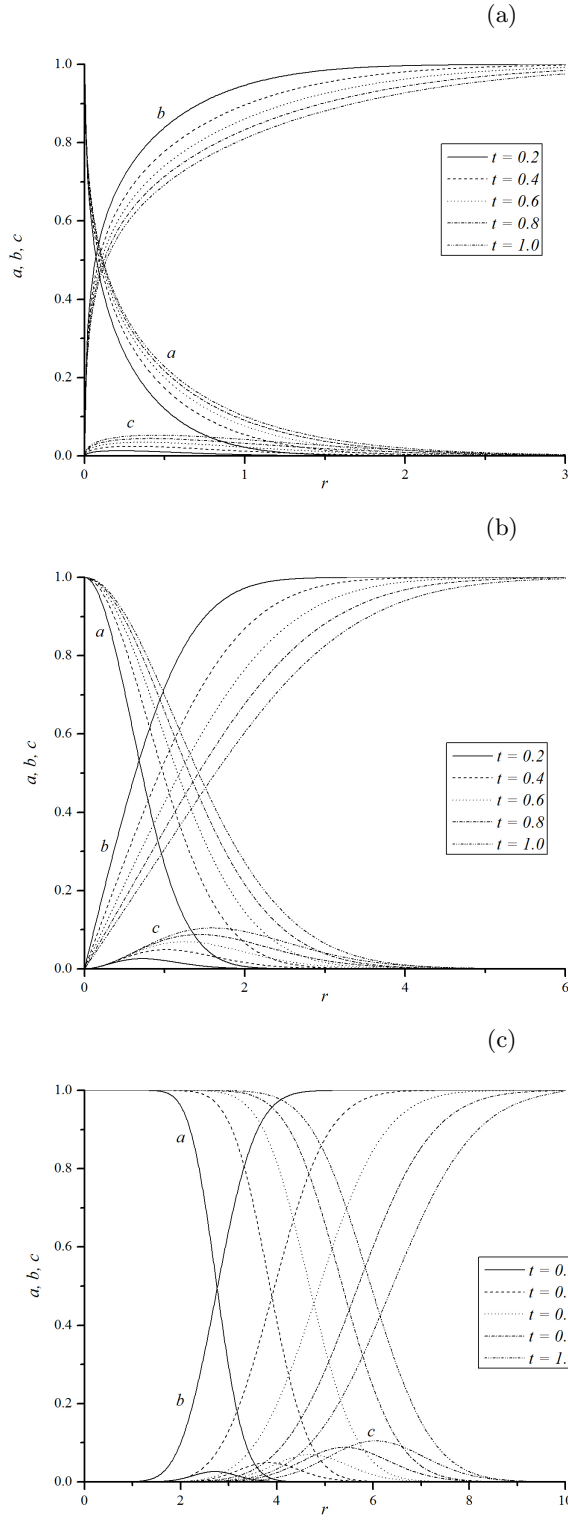


FIG. 1: Small time concentration profiles  $a$ ,  $b$  and  $c$  are plotted against  $r$  for (a)  $Pe = 0.1$ , (b)  $Pe = 1$  and (c)  $Pe = 10$ . In each case  $\delta_b = 0.5$ ,  $\varphi = \delta_c = 1$ .

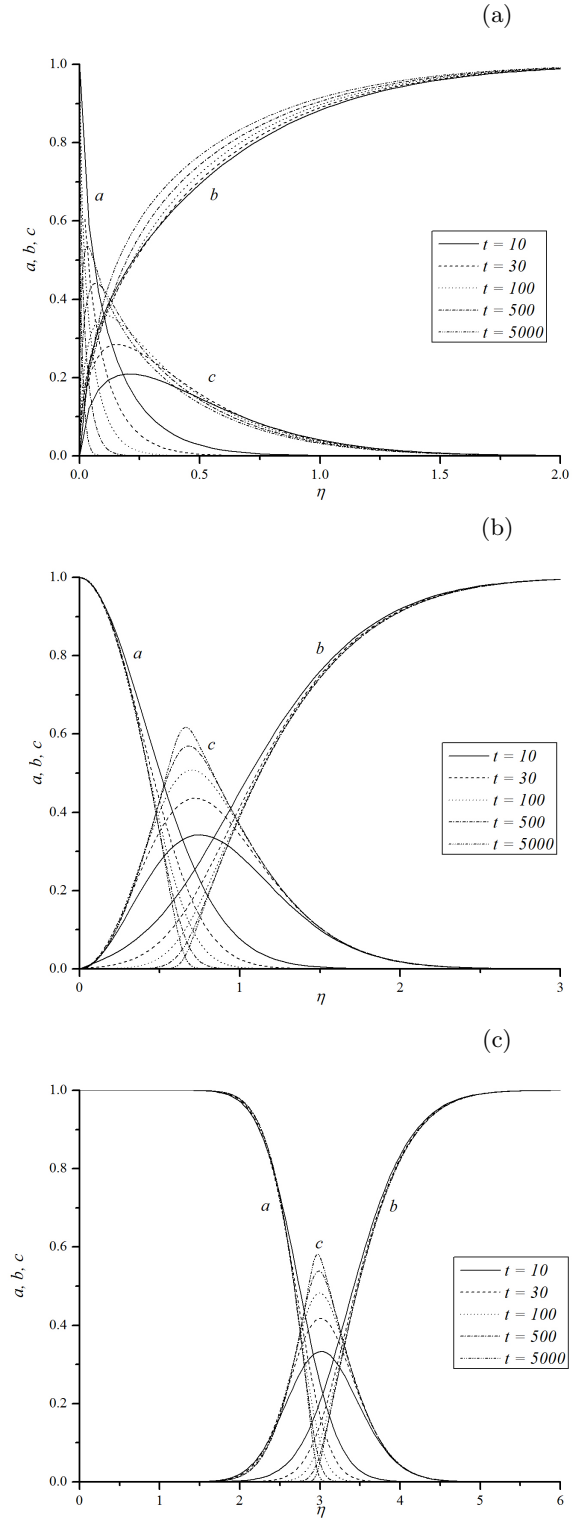


FIG. 2: Large time concentration profiles  $a$ ,  $b$  and  $c$  are plotted against  $\eta$  for (a)  $Pe = 0.1$ , (b)  $Pe = 1$  and (c)  $Pe = 10$ . In each case  $\delta_b = 0.5$ ,  $\varphi = \delta_c = 1$ .

front so that the concentration profiles resemble those associated with the planar reaction problem, but shifted to the right. Finally one notes that all of the results in figure 2 show the narrowing of the width of the reaction front in time when plotted against  $\eta$ .

#### IV. SMALL TIME ASYMPTOTIC SOLUTIONS

In the limit as  $\tau$  tends to zero the leading order transport equations in (7) for the reactants become:

$$-2\eta a_\eta + (2\text{Pe} - 1)\frac{a_\eta}{\eta} = a_{\eta\eta} \quad (8a)$$

$$-2\delta_b \eta b_\eta + (2\delta_b \text{Pe} - 1)\frac{b_\eta}{\eta} = b_{\eta\eta} \quad (8b)$$

with  $c = O(\tau)$ . Thus, to leading order, there is no product. The general solution to (8) take the form

$$a = d_1 + d_2 \Gamma(\text{Pe}, \eta^2), \quad b = d_3 + d_4 \Gamma(\delta_b \text{Pe}, \delta_b \eta^2)$$

where  $\Gamma$  is the incomplete Gamma function defined by

$$\Gamma(a, z) = \int_z^\infty x^{a-1} e^{-x} dx$$

see equation (6.5.3) in [29]. Note that the solution can also be written in terms of Whittaker's functions [30]. Using the 4 boundary conditions (7d) and (7e) leads to the solutions

$$a = \frac{\Gamma(\text{Pe}, \eta^2)}{\Gamma(\text{Pe})}, \quad (9a)$$

$$b = \varphi - \varphi \frac{\Gamma(\delta_b \text{Pe}, \delta_b \eta^2)}{\Gamma(\delta_b \text{Pe})}, \quad (9b)$$

where  $\Gamma(x) = \Gamma(0, x)$ . Now that the leading order analytical solutions have been determined in the small time asymptotic limit we can obtain some physical properties of the system.

##### A. Maximum reaction rate

We define the reaction rate as  $kab$ . The initial position of the reaction rate can be described as the point where the reaction rate is maximum, i.e. at  $(kab)_\eta = 0$ . Using the small time asymptotic solutions in equation (9) the maximum reaction rate is found to occur at

$$r_m = 2\beta\sqrt{t} \quad (10)$$

where  $\beta$  is the solution to the equation:

$$\frac{\Gamma(\delta_b \text{Pe}) - \Gamma(\delta_b \text{Pe}, \delta_b \beta^2)}{\Gamma(\text{Pe}, \beta^2)} = \delta_b^{\delta_b \text{Pe}} \beta^{2\text{Pe}(\delta_b - 1)} e^{(1 - \delta_b)\beta^2}. \quad (11)$$

Equivalently, the maximum reaction rate occurs at  $\eta = \beta$ . We note that, in dimensional quantities, the

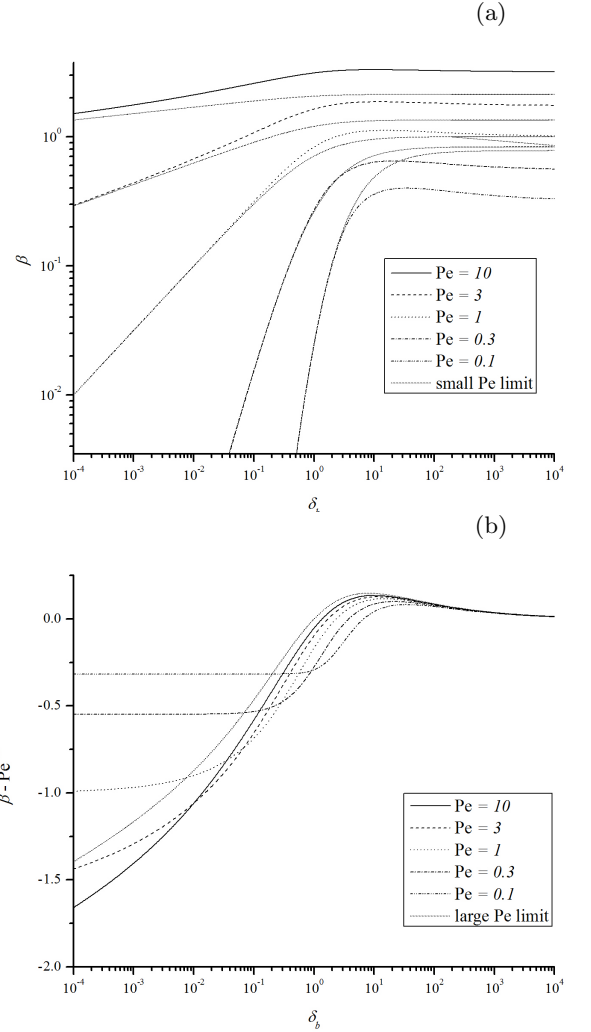


FIG. 3: The relationship between  $\beta$  and  $\delta_b$  for various values of  $\text{Pe}$  obtained from equation (11). In (a)  $\log_{10}(\delta_b)$  is plotted against  $\log_{10}(\beta)$  where the dotted lines denote the small  $\text{Pe}$  limit given analytically by equation (14). In (b)  $\log_{10}(\delta_b)$  is plotted against  $\beta - \sqrt{\text{Pe}}$  where the dotted line denotes the large  $\text{Pe}$  limit determined from equation (15).

position where the reaction rate is maximum is given by  $R_m = 2\beta\sqrt{D_A T}$ .

By numerically solving equation (11), the dependence of  $\beta$  on  $\delta_b$  can be determined, and is illustrated in figure 3 for various values of  $\text{Pe}$ . In figure 3(a), we observe that increasing  $\text{Pe}$  increases  $\beta$ , however,  $\beta$  has a non-monotonic dependence on  $\delta_b$ , just as in the planar reaction front case. In figure 3(b), we notice that  $\beta - \sqrt{\text{Pe}}$  is a non-monotonic function of both  $\text{Pe}$  and  $\delta_b$ , and thus so is the distance between the local maximum in the reaction rate and the contact line, as  $r_m - r_c = 2\sqrt{t}(\beta - \sqrt{\text{Pe}})$ . In the following subsections some limits are examined and additional properties of the reaction front are presented.

### B. Equal diffusion coefficients

If both reactants diffuse at the same rate, i.e.  $\delta_b = 1$ , then equation (11) simplifies to

$$\frac{\Gamma(\text{Pe}, \beta^2)}{\Gamma(\text{Pe})} = \frac{1}{2} \quad (12)$$

which reveals that  $\beta$  is a monotonic increasing function of  $\text{Pe}$ . This result is physically expected as increasing the flow rate increases the propagation of the reaction front. Using equation (B1) in Appendix B, in the large  $\text{Pe}$  limit we obtain

$$\beta \rightarrow \sqrt{\text{Pe}} - \frac{1}{6\sqrt{\text{Pe}}} + \mathcal{O}(\text{Pe}^{-3/2}) \quad (13)$$

so that the position of the reaction front quickly approaches the contact line.

### C. Slow flow rate

In the slow flow rate limit, i.e.  $\text{Pe}$  tending to zero, we shall also consider  $\beta$  small and  $\delta_b$  up to order unity. Using equations (A1) and (A2) in Appendix A we can expand equation (11) to first order in  $\text{Pe}$  and  $\beta$  to obtain

$$\beta \rightarrow \left( \frac{\delta_b \Gamma(\text{Pe} + 1)}{1 + \delta_b} \right)^{1/(2\text{Pe})} \quad (14)$$

which tends to zero very quickly. This equation reveals that increasing  $\delta_b$  or  $\text{Pe}$  lead to an increase in  $\beta$ . This asymptotic analytical solution (14) is illustrated by the dotted lines in figure 3(a) and found to be in good agreement with the numerical solution of equation (11) when both  $\text{Pe}$  and  $\beta$  are small. If  $\delta_b \gg 1$  then  $\beta$  may no longer be small and then the limit fails.

### D. Fast flow rate

In the fast flow rate limit, i.e.  $\text{Pe}$  tending to infinity, we choose a variable proportional to the distance between the reaction zone and the contact line by writing  $\chi = \sqrt{2}(\beta - \sqrt{\text{Pe}})$ . Using the zeroth order term from equation (B1) and (B2) in Appendix B along with  $e^{-xyz}(1 + x/z)^{yz^2} \rightarrow e^{-yx^2/2}$  as  $z$  tends to infinity equation (11) becomes

$$e^{(\delta_b - 1)\chi^2} \text{erfc}(-\sqrt{\delta_b}\chi) = \sqrt{\delta_b} \text{erfc}(\chi) \quad (15)$$

to leading order. In figure 3(b) the numerical solution to  $\chi$  from equation (15) allows the determination of  $\beta$  and is illustrated by the dotted lines. For large  $\text{Pe}$ , this solution is found to be in good agreement with the numerical solution of (11) when  $\delta_b$  is not too small.

We note that equation (15) is the same equation as for planar reaction fronts obtained by Koza [16] in the

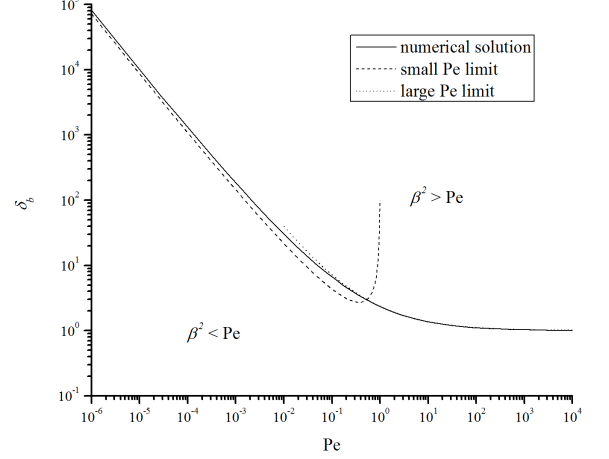


FIG. 4: The condition for the initial reaction front to be located at the fluid contact line in the  $(\delta_b, \text{Pe})$  parameter space, obtained from equation (16). The dotted and dashed lines are the small and large  $\text{Pe}$  limits given by equations (17a) and (17b), respectively.

small time asymptotic limit. Thus we have shown that  $r_m = r_c + x_m/\sqrt{2}$  where  $x_m$  is the location where the reaction rate is maximum for a planar reaction front. Using the properties of equation (15) we find that

$$\beta \rightarrow \sqrt{\text{Pe}} + \frac{\sqrt{\pi}(\sqrt{\delta_b} - 1)}{4\sqrt{2}\delta_b}$$

for  $|\delta_b - 1| \ll 1$ , so that the reaction front is only ahead of the contact line when  $\delta_b > 1$ . Further, one finds that the position of the reaction front varies non-monotonically with  $\delta_b$ , such that the reaction front extends furthest ahead of the contact line when  $\delta_b = \delta_b^{(c)} \approx 8.056588$ , in dimensionless variables. In dimensional variables this means that, for a fixed value of  $D_A$ , the reaction fronts extends furthest ahead of the contact line when  $D_B = D_A/\delta_b^{(c)}$ , and by symmetry, for a fixed value of  $D_B$ , the reaction front lags furthest behind the contact line when  $D_B = \delta_b^{(c)} D_A$ .

### E. Reaction Front at Contact line

When the reaction front is located at the contact line we have  $\beta = \sqrt{\text{Pe}}$  and equation (11) becomes:

$$\frac{\Gamma(\delta_b \text{Pe}) - \Gamma(\delta_b \text{Pe}, \delta_b \text{Pe})}{\Gamma(\text{Pe}, \text{Pe})} = \delta_b^{\delta_b \text{Pe}} (\text{Pe}/e)^{\text{Pe}(\delta_b - 1)}. \quad (16)$$

By numerically solving equation (16) the parameter values of  $\text{Pe}$  and  $\delta_b$  required for the initial reaction front to be located at the fluid contact line is obtained, and plotted in figure 4. We notice that if  $\delta_b$  is greater than a critical value greater than unity and depending on  $\text{Pe}$ ,

then  $\beta^2 > \text{Pe}$  and the reaction front will travel ahead of the contact line. Thus when  $\delta_b < 1$ , then  $\beta < \sqrt{\text{Pe}}$  for all  $\text{Pe} > 0$ . Increasing  $\text{Pe}$  is found to increase  $\beta$  and reduces the critical value of  $\delta_b$  required for which  $\beta = \sqrt{\text{Pe}}$ . Below this critical value of  $\delta_b$ , increasing  $\delta_b$  increases  $\beta$ , whilst above this value  $\beta$  has the same type of non-monotonic dependence on  $\delta_b$  as found in planar reaction fronts.

Using equations (A1) and (A2) in Appendix A, we find that as  $\text{Pe}$  tends to zero, we require that  $\delta_b$  tends to infinity in order to maintain the reaction front at the contact line. Keeping the most dominant terms in the expansion, we obtain

$$\delta_b \rightarrow -\frac{1}{\text{Pe} \ln(\text{Pe})} \quad (17a)$$

which is in reasonable agreement with the numerical solution to equation (16), see figure 4.

In the fast flow rate limit, taking  $\text{Pe} \rightarrow \infty$  and using equations (B1) and (B2) in Appendix B yields

$$\delta_b \rightarrow 1 + \frac{4\sqrt{2}}{3\sqrt{\pi}\text{Pe}} + \frac{8}{9\pi\text{Pe}} + \dots \quad (17b)$$

which is found to be in very good agreement with the numerical solution to equation (16) as shown in figure 4.

## F. First moment of the reaction rate

In the previous section the small time asymptotic location of the position where the reaction rate has a maximum was analyzed. Another interesting case to examine is the first moment of the reaction rate. In radial coordinates this definition becomes

$$r_f = \frac{\int_0^\infty ab r^2 dr}{\int_0^\infty ab r dr} = 2\sqrt{t} \frac{\int_0^\infty ab \eta^2 d\eta}{\int_0^\infty ab \eta d\eta}. \quad (18)$$

Using the small time asymptotic profiles in equation (9) we can obtain  $r_f$ , see figure 5(a). Figure 5(a) shows that  $r_f$  is a monotonic increasing function of both  $\delta_b$  and  $\text{Pe}$ . Figure 5(b) shows that the term  $r_f - r_c$  is a monotonic increasing function of  $\delta_b$  and it is a monotonic decreasing function of  $\text{Pe}$ . We note that  $r_f$  can be expressed analytically in terms of hypergeometric functions, but here we will only present it analytically in the fast flow rate limit.

In the fast flow rate regime, using equation (B1), the solutions in equation (9), to second order, are given by

$$a = \frac{\text{erfc}(\xi)}{2} + \frac{e^{-\xi^2}}{6\sqrt{\pi}} \left[ \frac{\xi^2 - 2}{\sqrt{2\text{Pe}}} + \frac{6\xi - 8\xi^3 + \xi^5}{12\text{Pe}} \right] \quad (19a)$$

$$b = \frac{\varphi \text{erfc}(-\sqrt{\delta_b} \xi)}{2} - \frac{\varphi e^{-\delta_b \xi^2}}{6\sqrt{\pi} \delta_b} \left[ \frac{\delta_b \xi^2 - 2}{\sqrt{2\text{Pe}}} + \frac{6\xi - 8\delta_b \xi^3 + \delta_b^2 \xi^5}{12\text{Pe}} \right] \quad (19b)$$

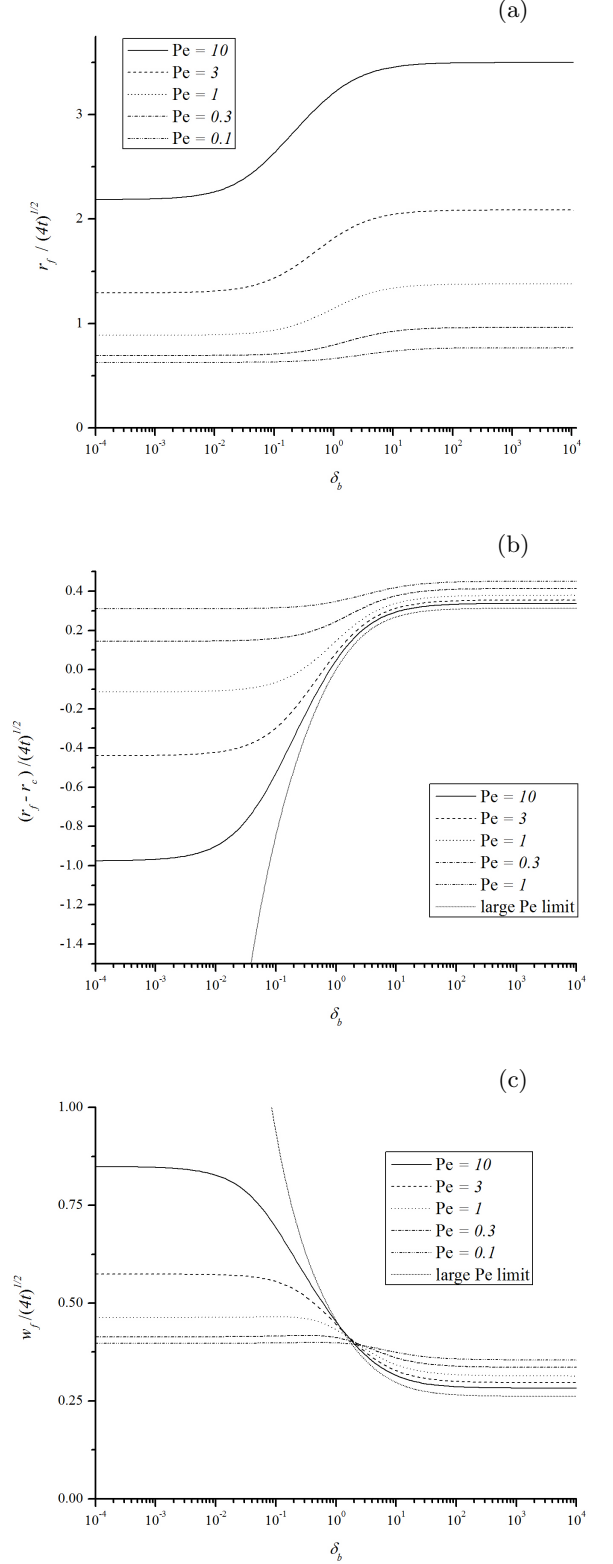


FIG. 5: The relationship between small time asymptotic values of (a)  $r_f$ , (b)  $r_f - r_c$  and (c)  $w_f$  with  $\delta_b$  for various values of  $\text{Pe}$ . The dotted line in (b) is the large  $\text{Pe}$  limit of  $r_f - r_c$  given by equation (20) and in (c) the dotted line is the large  $\text{Pe}$  limit of  $w_f$  given by equation (22).



where  $\xi = \sqrt{2}(\eta - \sqrt{\text{Pe}})$ . Substituting these solutions into equation (18) and expanding in large Pe allows  $r_f$  to be evaluated analytically as:

$$r_f \rightarrow 2\sqrt{\text{Pe}t} + \frac{\sqrt{\pi t}(\delta_b - 1)}{2\sqrt{2\delta_b(1 + \delta_b)}} + O(\text{Pe}^{-1/2}) \quad (20)$$

to leading order, where the integral results in [22] have been used. One notes that  $r_f$  monotonically increases with  $\delta_b$ , unlike  $r_m$ , and  $r_f$  coincides with the location of the contact line  $r_c$  when  $\delta_b = 1$ . Additionally, we have obtained  $r_f = r_c + x_f/\sqrt{2}$  where  $x_f$  is the solution given by equation (16) in [22].

### G. Width of the reaction front

The width of the reaction front is generally obtained using the second moment of the reaction rate. Here we define the width of the reaction front as

$$\begin{aligned} w_f^2 &= \frac{\int_0^\infty ab(r - r_f)^2 r dr}{\int_0^\infty ab r dr} = \frac{\int_0^\infty ab r^3 dr}{\int_0^\infty ab r dr} - r_f^2 \\ &= 4t \frac{\int_0^\infty ab \eta^3 d\eta}{\int_0^\infty ab \eta d\eta} - r_f^2. \end{aligned} \quad (21)$$

Using the small time asymptotic profiles in equation (9) we can obtain  $w_f$ , see figure 5(c), which shows that  $w_f$  is a monotonic decreasing function of  $\delta_b$ , but surprisingly the effect of Pe is non-monotonic. If  $\delta_b$  is large then increasing Pe reduces  $w_f$ , however, if  $\delta_b$  is small then increasing Pe increases  $w_f$ . Similarly, we can express  $w_f$  analytically in terms of hypergeometric functions, but here we will just present the solution in the fast flow rate limit.

Substituting the solutions in equation (19) into equation (21) and expanding in large Pe allows  $w_f$  to be evaluated analytically as:

$$w_f^2 \rightarrow \frac{t}{\delta_b + 1} \left[ \left( \frac{1}{\delta_b} + \delta_b \right) \left( \frac{2}{3} - \frac{\pi}{8} \right) + \frac{1}{3} + \frac{\pi}{4} \right] \quad (22)$$

to leading order. This expression for  $w_f^2$  is exactly  $\frac{1}{2}$  of the value one obtains for a planar reaction front, see (18) in [22], and thus the small time asymptotic width of a radial reaction front in the large Pe limit is  $1/\sqrt{2}$  of the width of the corresponding planar reaction front.

### H. Summary of Small time asymptotic properties

We have found that increasing Pe has a monotonic increasing effect on both  $r_m$  and  $r_f$ , a monotonic decreasing effect on  $r_f - r_c$ , and a non-monotonic effect on  $r_m - r_c$  and  $w_f$ . The parameter  $\delta_b$  has a monotonic increasing effect on  $r_f$  and  $r_f - r_c$ , a monotonic decreasing effect on  $w_f$  and a non-monotonic effect on  $r_m$  and  $r_m - r_c$ . These results are summarized in Table I. Finally we note that

TABLE I: Parameter effects upon the small time asymptotic properties of the reaction front.

Parameter	$r_m$	$r_m - r_c$	$r_f$	$r_f - r_c$	$w_f$
$\delta_b$	$\pm$	$\pm$	$+$	$+$	$-$
Pe	$+$	$\pm$	$+$	$-$	$\pm$

increasing  $\delta_b$  or increasing Pe, when  $\delta_b > 1$ , sufficiently lead to  $r_m > r_c$ . Now that the various properties of the small time asymptotic solutions have been obtained, in the next section the properties of the large time asymptotic solutions will be examined.

## V. LARGE TIME ASYMPTOTIC OUTER SOLUTIONS

In the large time limit, we seek a similarity solution outside the reaction zone where the solution does not depend on  $\tau$  and  $ab = 0$ , i.e. away from the reaction front, which we name the outer solution. These assumptions reduce the equations in (7) to

$$-2\eta a_\eta + (2\text{Pe} - 1) \frac{a_\eta}{\eta} = a_{\eta\eta} \quad (23a)$$

$$-2\delta_b \eta b_\eta + (2\delta_b \text{Pe} - 1) \frac{b_\eta}{\eta} = b_{\eta\eta} \quad (23b)$$

$$-2\delta_c \eta c_\eta + (2\delta_c \text{Pe} - 1) \frac{c_\eta}{\eta} = c_{\eta\eta}. \quad (23c)$$

We assume that the reaction front is located at

$$r_f = 2\alpha\sqrt{t}, \quad (24)$$

which is equivalent to  $\eta = \alpha$ . We now introduce the superscript notation 1 and 2 to denote the outer solution behind and ahead of the reaction front, respectively. At the reaction front we suppose that

$$a^{(1)} = b^{(2)} = 0, \quad c^{(1)} = c^{(2)} = W \quad \text{at} \quad \eta = \alpha.$$

Using these 4 boundary conditions along with equations (7d) and (7e) yield the solutions

$$a^{(1)} = \frac{\Gamma(\text{Pe}, \eta^2) - \Gamma(\text{Pe}, \alpha^2)}{\Gamma(\text{Pe}) - \Gamma(\text{Pe}, \alpha^2)}, \quad b^{(1)} = 0 \quad (25a)$$

$$b^{(2)} = \varphi - \varphi \frac{\Gamma(\delta_b \text{Pe}, \delta_b \eta^2)}{\Gamma(\delta_b \text{Pe}, \delta_b \alpha^2)}, \quad a^{(2)} = 0 \quad (25b)$$

$$c^{(1)} = W \frac{\Gamma(\delta_c \text{Pe}) - \Gamma(\delta_c \text{Pe}, \delta_c \eta^2)}{\Gamma(\delta_c \text{Pe}) - \Gamma(\delta_c \text{Pe}, \delta_c \alpha^2)}, \quad (25c)$$

$$c^{(2)} = W \frac{\Gamma(\delta_c \text{Pe}, \delta_c \eta^2)}{\Gamma(\delta_c \text{Pe}, \delta_c \alpha^2)}. \quad (25d)$$

However, the values of  $\alpha$  and  $W$  have not yet been determined. These quantities are obtained by matching the reactant fluxes across the reaction zone, namely, using

$$-\frac{\partial a^{(1)}}{\partial \eta} = \frac{1}{\delta_b} \frac{\partial b^{(2)}}{\partial \eta} = \frac{1}{\delta_c} \frac{\partial (c^{(1)} - c^{(2)})}{\partial \eta} \quad \text{at} \quad \eta = \alpha. \quad (26)$$

By writing

$$\begin{aligned}
 U &= -\frac{\partial a^{(1)}}{\partial \eta} = \frac{2\alpha^{2\text{Pe}-1}e^{-\alpha^2}}{\Gamma(\text{Pe}) - \Gamma(\text{Pe}, \alpha^2)}, \\
 V &= \frac{\partial b^{(2)}}{\partial \eta} = \frac{2\varphi\delta_b^{\delta_b\text{Pe}}\alpha^{2\delta_b\text{Pe}-1}e^{-\delta_b\alpha^2}}{\Gamma(\delta_b\text{Pe}, \delta_b\alpha^2)}, \\
 W_L &= \frac{\partial c^{(1)}}{\partial \eta} = \frac{2W\delta_c^{\delta_c\text{Pe}}\alpha^{2\delta_c\text{Pe}-1}e^{-\delta_c\alpha^2}}{\Gamma(\delta_c\text{Pe}) - \Gamma(\delta_c\text{Pe}, \delta_c\alpha^2)}, \\
 W_R &= -\frac{\partial c^{(2)}}{\partial \eta} = \frac{2W\delta_c^{\delta_c\text{Pe}}\alpha^{2\delta_c\text{Pe}-1}e^{-\delta_c\alpha^2}}{\Gamma(\delta_c\text{Pe}, \delta_c\alpha^2)}
 \end{aligned}$$

equation (26) becomes

$$U = \frac{V}{\delta_b} = \frac{W_R + W_L}{\delta_c}$$

which leads to the equations

$$\frac{\Gamma(\delta_b\text{Pe}, \delta_b\alpha^2)}{\Gamma(\text{Pe}) - \Gamma(\text{Pe}, \alpha^2)} = \varphi\delta_b^{\delta_b\text{Pe}-1}\alpha^{2\text{Pe}(\delta_b-1)}e^{\alpha^2(1-\delta_b)} \quad (27)$$

and

$$\begin{aligned}
 W &= \frac{\Gamma(\delta_c\text{Pe}, \delta_c\alpha^2) [\Gamma(\delta_c\text{Pe}) - \Gamma(\delta_c\text{Pe}, \delta_c\alpha^2)]}{\Gamma(\delta_c\text{Pe}) [\Gamma(\text{Pe}) - \Gamma(\text{Pe}, \alpha^2)]} \\
 &\times \alpha^{2\text{Pe}(1-\delta_c)}e^{\alpha^2(\delta_c-1)}\delta_c^{1-\delta_c\text{Pe}}. \quad (28)
 \end{aligned}$$

Thus, once equation (27) has been solved,  $W$  and hence the outer solution have been determined.

By numerically solving equation (27), the dependence of  $\alpha$  on  $\delta_b$ ,  $\text{Pe}$  and  $\varphi$  can be determined. In figure 6 the variation of  $\alpha$  with  $\delta_b$  is illustrated for various values of  $\text{Pe}$  when  $\varphi = 1$ . In figure 6(a), we observe that increasing  $\text{Pe}$  or  $\delta_b$  increases  $\alpha$ . In figure 6(b), we notice that the distance between the reaction front and the contact line, i.e.  $r_f - r_c = 2\sqrt{t}(\alpha - \sqrt{\text{Pe}})$ , is a monotonic increasing function of  $\delta_b$  and a non-monotonic function of  $\text{Pe}$ .

In figure 7 the variation of  $\alpha$  with  $\delta_b$  is illustrated for various values of  $\varphi$  when  $\text{Pe}=1$ . We observe that decreasing  $\varphi$  or increasing  $\delta_b$  increases  $\alpha$ . In the following subsections some interesting limits are examined and additional properties of the reaction front are presented.

#### A. Equal diffusion coefficients

If both reactants diffuse at the same rate so that  $\delta_b = 1$  then equation (27) reduces to

$$\frac{\varphi}{1+\varphi} = \frac{\Gamma(\text{Pe}, \alpha^2)}{\Gamma(\text{Pe})} \quad (29)$$

which reveals that  $\alpha$  is a monotonic decreasing function of  $\varphi$ . Further, an expansion in large  $\text{Pe}$  yields

$$\alpha \rightarrow \sqrt{\text{Pe}} + \frac{1}{\sqrt{2}}\text{erfc}^{-1}\left(\frac{2\varphi}{1+\varphi}\right) \quad (30)$$

which is found to be in good agreement with numerical solutions to equation (29) when  $\text{Pe}$  is large.

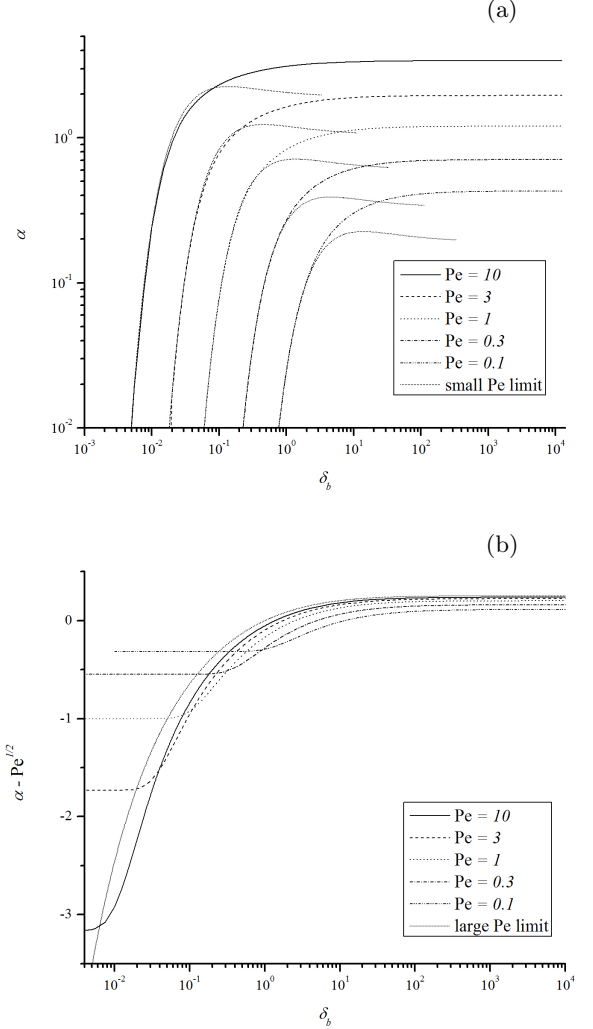


FIG. 6: The relationship between  $\alpha$  and  $\delta_b$  for various values of  $\text{Pe}$  obtained from equation (27) when  $\varphi = 1$ . In (a)  $\log_{10}(\delta_b)$  is plotted against  $\log_{10}(\alpha)$  where the dotted lines denote the small  $\text{Pe}$  limit given by equation (31). In (b)  $\log_{10}(\delta_b)$  is plotted against  $\alpha - \sqrt{\text{Pe}}$  where the dotted line denotes the large  $\text{Pe}$  limit determined from equation (32).

#### B. Slow flow rate

Letting  $\text{Pe}$  tend to zero and assuming that  $\alpha$  is small with  $\varphi$  and  $\delta_b$  both being  $O(1)$ , to leading order yields

$$\alpha \rightarrow \frac{1}{\sqrt{\delta_b}} \left( \frac{\Gamma(\delta_b\text{Pe} + 1)}{\varphi + 1} \right)^{1/(2\delta_b\text{Pe})} \quad (31)$$

which tends to zero very quickly as  $\text{Pe}$  tends to zero. This analytical solution (31) is illustrated by the dotted lines in figure 6(a) and is found to be in good agreement with the actual numerical solution when both  $\text{Pe}$  and  $\alpha$  are small, however, the approximation is not valid when the term  $\text{Pe}\delta_b$  becomes large as the approximation predicts that  $\alpha$  has a non-monotonic dependence on  $\delta_b$  but the ac-

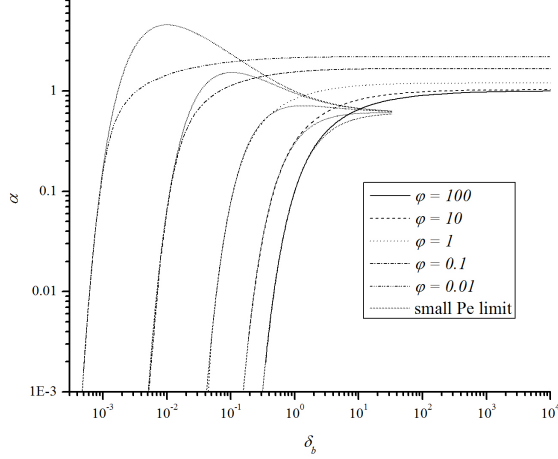


FIG. 7: The relationship between  $\alpha$  and  $\delta_b$  for various values of  $\varphi$  obtained from equation (27) when  $Pe = 1$ . The dotted lines denote the small  $Pe$  limit by equation (31).

tual solution shows that increasing  $\delta_b$  causes a monotonic increase in  $\alpha$ .

In figure 7 we find that the approximation can be good even when  $Pe$  is not small, when  $\delta_b \ll 1$ , however, if  $\varphi$  is small then the approximation starts to diverge from the numerical solution at smaller values of  $\delta_b$ .

### C. Fast flow rate

Letting  $Pe$  tend to infinity allows equation (27) to be reduced to the same equation as for planar reaction fronts obtained by Koza [16]. By writing  $\psi = \sqrt{2}(\alpha - \sqrt{Pe})$ , to leading order, we obtain

$$e^{(\delta_b-1)\psi^2} \operatorname{erfc}(\sqrt{\delta_b}\psi) = \frac{\varphi}{\sqrt{\delta_b}} \operatorname{erfc}(-\psi) \quad (32)$$

whose properties have already been studied in the literature for the planar reaction front.

In figure 6(b) the numerical solution to  $\psi$  from equation (32) allows the determination of  $\alpha$  and is illustrated by the dotted line. For large  $Pe$ , this solution is found to be in good agreement with the numerical solution of (27) when  $\delta_b$  is not too small.

### D. Reaction Front at Contact Line

When the reaction front is located at the contact line we have  $\alpha = \sqrt{Pe}$  and equation (27) becomes:

$$\frac{\Gamma(\delta_b Pe, \delta_b Pe)}{\Gamma(Pe) - \Gamma(Pe, Pe)} = \varphi \delta_b^{\delta_b Pe - 1} (Pe/e)^{Pe(\delta_b - 1)}. \quad (33)$$

By numerically solving equation (33) the parameter values of  $Pe$  and  $\delta_b$  required for the large time asymptotic

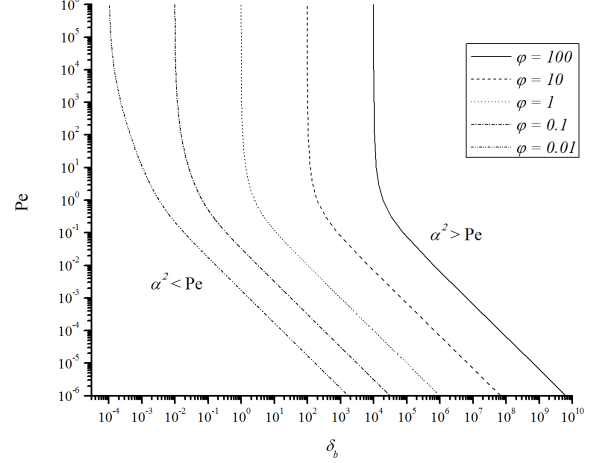


FIG. 8: The condition for the large time asymptotic position of the reaction front to be located at the fluid contact line in the  $(\delta_b, Pe)$  parameter space for various values of  $\varphi$ , obtained from equation (33).

position of the reaction front to be located at the fluid contact line is obtained for various values of  $\varphi$ , and plotted in figure 8. We notice that if  $\delta_b$  is greater than a critical value greater than  $1/\varphi^2$  and depending on  $Pe$ , then  $\alpha^2 > Pe$  and the reaction front will travel ahead of the contact line. Thus when  $\delta_b < \varphi$ , then  $\alpha < \sqrt{Pe}$  for all  $Pe > 0$ . Increasing  $Pe$  is found to increase  $\alpha$  and reduces the critical value of  $\delta_b$  required for which  $\alpha = \sqrt{Pe}$ .

Using equations (A1) and (A2) in Appendix A, we find that as  $Pe$  tends to zero, we require that  $\delta_b$  tends to infinity in order to maintain the reaction front at the contact line. Keeping the most dominant terms in the expansion, we obtain  $\varphi \rightarrow e^{\delta_b Pe} (\delta_b Pe)^{1-\delta_b Pe} \Gamma(\delta_b Pe, \delta_b Pe)$ . If  $\varphi \gg 1$  and  $Pe$  tends to zero then we find that

$$\delta_b \rightarrow \frac{2}{\pi Pe} \left( \varphi + \frac{1}{3} \right)^2 \quad (34a)$$

which is in reasonable agreement with the numerical solution to equation (33), see figure 8, when  $Pe$  is small.

In the fast flow rate limit, taking  $Pe \rightarrow \infty$  and using equations (B1) and (B2) in Appendix B yields

$$\varphi = \sqrt{\delta_b} - \frac{\sqrt{2}(1 + \sqrt{\delta_b})}{3\sqrt{\pi Pe}} + \frac{1 + \sqrt{\delta_b}}{9\pi Pe} + \frac{\delta_b - 1}{12\sqrt{\delta_b} Pe} \quad (34b)$$

which is found to be in very good agreement with the numerical solution to equation (33), as shown in figure 8, when  $Pe$  is large. The first term of equation (34b) is  $\varphi = \sqrt{\delta_b}$  which is equivalent to the condition obtained by Koza (1996) for the case of a stationary planar reaction front, namely

$$\frac{B_0 \sqrt{D_B}}{A_0 \sqrt{D_A}} = 1.$$

### E. Total amount of the product

The total amount of product produced in dimensional quantities is

$$\begin{aligned} C_{total} &= \int_0^{2\pi} \int_0^\infty CRdRd\theta = 2\pi A_0 L_0^2 \int_0^\infty crdr \\ &= 8\pi A_0 L_0^2 t \int_0^\infty c\eta d\eta = 8\pi A_0 D_A T I_0 \end{aligned}$$

so that the production rate is linear in time where

$$I_0 = \int_0^\infty c\eta d\eta.$$

This can be evaluated using the large time asymptotic solutions for  $c_1$  and  $c_2$  in (25). Using

$$\int_0^x \Gamma(a, z) dz = (x - a)\Gamma(a, x) - x^a e^{-x} + \Gamma(a + 1)$$

we find that

$$I_0 = \int_0^\infty c\eta d\eta = \frac{e^{-\alpha^2} \alpha^{2Pe}}{2[\Gamma(Pe) - \Gamma(Pe, \alpha^2)]} = \frac{UPe}{4}.$$

If  $\alpha$  is considered fixed then the production rate increases as  $Pe$  is increased. If  $Pe$  is considered fixed then the production rate decreases as  $\alpha$  is increased.

Returning to dimensional quantities we have

$$C_{total} = \frac{4\pi A_0 D_A T e^{-\alpha^2} \alpha^{2Pe}}{\Gamma(Pe) - \Gamma(Pe, \alpha^2)} = \frac{A_0 U Q T}{2}. \quad (35)$$

We plot the total amount of the product against  $\delta_b$  for various values of  $Pe$  when  $\varphi = 1$  in figure 9 and the total amount of the product against  $\delta_b$  for various values of  $\varphi$  when  $Pe = 1$  in figure 10.

### VI. LARGE TIME ASYMPTOTIC INNER SOLUTIONS

We now investigate the inner solution, which is only valid inside the reaction zone, i.e. only around the reaction front. We introduce the inner coordinate  $Z = (\eta - \alpha)\tau^\sigma$  where  $\sigma > 0$  so that as  $\tau$  tends to infinity the term  $Z/\tau^\sigma$  tends to zero corresponding to  $\eta$  tending to  $\alpha$ . Expanding the outer solutions around the reaction front, namely,  $\eta = \alpha$ , we obtain

$$\begin{aligned} a_L &\rightarrow -\frac{UZ}{\tau^\sigma}, \quad b_L \rightarrow 0, \quad c_L \rightarrow W + \frac{W_L Z}{\tau^\sigma}, \\ a_R &\rightarrow 0, \quad b_R \rightarrow \frac{VZ}{\tau^\sigma}, \quad c_R \rightarrow W - \frac{W_R Z}{\tau^\sigma}. \end{aligned}$$

We now seek an inner solution in a form that can match the outer solution by writing

$$a_I = \frac{\mathcal{A}^1(Z)}{\tau^\sigma}, \quad b_I = \frac{\mathcal{B}^1(Z)}{\tau^\sigma}, \quad c_I = W + \frac{\mathcal{C}^1(Z)}{\tau^\sigma}.$$

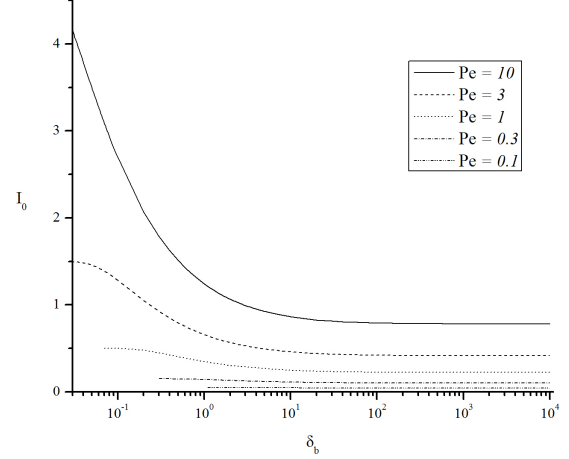


FIG. 9: The relationship between the total amount of the product  $I_0$  and  $\delta_b$  for various values of  $Pe$  with  $\varphi = 1$ .

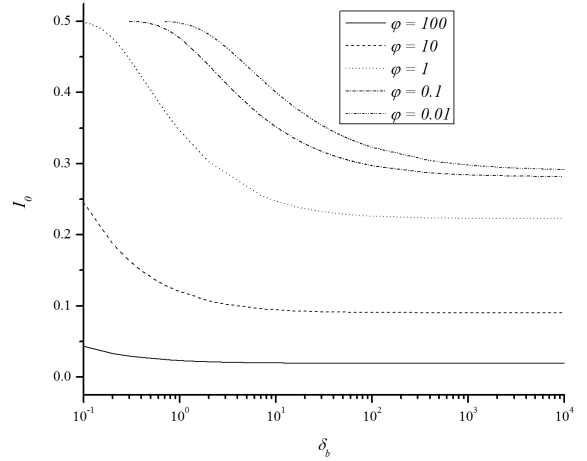


FIG. 10: The relationship between the total amount of the product  $I_0$  and  $\delta_b$  for various values of  $\varphi$  with  $Pe = 1$ .

Substituting these expressions into system (7) yields

$$\begin{aligned} &\sigma \mathcal{A}^1 \tau^{-2\sigma} + \frac{1}{2}((1 - 2\sigma)Z\tau^{-2\sigma} + \alpha\tau^{-\sigma})\mathcal{A}_Z^1 \\ &- \frac{(2Pe - 1)\tau^{-\sigma}\mathcal{A}_Z^1}{4(\alpha + Z\tau^{-\sigma})} = -\frac{\mathcal{A}_{ZZ}^1}{4} + \tau^{1-3\sigma}\mathcal{A}^1\mathcal{B}^1, \end{aligned} \quad (36a)$$

$$\begin{aligned} &\sigma \mathcal{B}^1 \tau^{-2\sigma} + \frac{1}{2}((1 - 2\sigma)Z\tau^{-2\sigma} + \alpha\tau^{-\sigma})\mathcal{B}_Z^1 \\ &- \frac{(2\delta_b Pe - 1)\tau^{-\sigma}\mathcal{B}_Z^1}{4\delta_b(\alpha + Z\tau^{-\sigma})} = -\frac{\mathcal{B}_{ZZ}^1}{4\delta_b} + \tau^{1-3\sigma}\mathcal{A}^1\mathcal{B}^1, \end{aligned} \quad (36b)$$

$$\begin{aligned} &\sigma \mathcal{C}^1 \tau^{-2\sigma} + \frac{1}{2}((1 - 2\sigma)Z\tau^{-2\sigma} + \alpha\tau^{-\sigma})\mathcal{C}_Z^1 \\ &- \frac{(2\delta_c Pe - 1)\tau^{-\sigma}\mathcal{C}_Z^1}{4\delta_c(\alpha + Z\tau^{-\sigma})} = -\frac{\mathcal{C}_{ZZ}^1}{4\delta_c} - \tau^{1-3\sigma}\mathcal{A}^1\mathcal{B}^1. \end{aligned} \quad (36c)$$

In the large time evolution, these equations consist of terms whose coefficients are powers of  $\tau$ . In each equation the powers of  $\tau$  present are  $-2\sigma$ ,  $-\sigma$ ,  $0$  and  $1-3\sigma$ . As  $\sigma > 0$ , we have  $\sigma = 1/3$ . The leading order equations are

$$\mathcal{A}_{ZZ}^1 = \frac{\mathcal{B}_{ZZ}^1}{\delta_b} = -\frac{\mathcal{C}_{ZZ}^1}{\delta_c} = 4\mathcal{A}^1\mathcal{B}^1.$$

The matching conditions for the inner solution with the left and right outer solutions are

$$\begin{aligned} \mathcal{A}^1 &\rightarrow -UZ, & \mathcal{B}^1 &\rightarrow 0, & \mathcal{C}^1 &\rightarrow W_L Z, & \text{as } Z \rightarrow -\infty, \\ \mathcal{A}^1 &\rightarrow 0, & \mathcal{B}^1 &\rightarrow VZ, & \mathcal{C}^1 &\rightarrow -W_R Z, & \text{as } Z \rightarrow \infty. \end{aligned}$$

By integrating the leading order equation with respect to  $Z$  twice and using the conditions as  $Z \rightarrow -\infty$  we obtain

$$\mathcal{A}^1 + UZ = \frac{\mathcal{B}^1}{\delta_b} = \frac{W_L Z - \mathcal{C}^1}{\delta_c}$$

then the condition as  $Z \rightarrow +\infty$  leads to

$$U = \frac{V}{\delta_b} = \frac{W_L + W_R}{\delta_c}$$

which is identical to the equation obtained in section V by balancing the fluxes on each side of the reaction front.

Hence, we have shown that  $\mathcal{B}^1 = \delta_b (\mathcal{A}^1 + UZ)$  and  $\mathcal{C}^1 = W_L Z - \delta_c (\mathcal{A}^1 + UZ)$ . Then using  $\mathcal{A}_{ZZ}^1 = 4\mathcal{A}^1\mathcal{B}^1$  we obtain a single ode for  $\mathcal{A}^1$  given by  $\mathcal{A}_{ZZ}^1 = 4\delta_b\mathcal{A}^1 (\mathcal{A}^1 + UZ)$ . By scaling  $Z = (4\delta_b U)^{-1/3}z$  and  $\mathcal{A}^1 = (4\delta_b/U^2)^{-1/3}G$  we obtain

$$G_{zz} = G(z + G). \quad (37a)$$

The boundary conditions become

$$G \rightarrow -z \quad \text{as } z \rightarrow -\infty, \quad (37b)$$

$$G \rightarrow 0 \quad \text{as } z \rightarrow +\infty. \quad (37c)$$

The inner solution  $G$  can then be obtained numerically using equation (37). Once  $G$  has been obtained we have  $\mathcal{A}^1 = (4\delta_b/U^2)^{-1/3}G$ ,  $\mathcal{B}^1 = (4/\delta_b^2 U^2)^{-1/3}(G + z)$  and  $\mathcal{C}^1 = -\delta_c(4\delta_b/U^2)^{-1/3}[G + z - zW_L/(U\delta_c)]$ . System (37) was analyzed by [13] who found that  $G(-z) \equiv G(z) + z$  so that the differential equation in (37) can be written as  $G_{zz} = G(z)G(-z)$  so that  $G_{zzz} = 0$  at  $z = 0$  and thus  $G_{zz}$  is maximum at  $z = 0$ .

#### A. First moment of the reaction rate

We note that the reaction rate  $ab$  can be written as  $\delta_b^{1/3}UG(G+z)/(4t)^{2/3}$ . Now let's consider the first moment of the reaction rate

$$\frac{r_f}{2\sqrt{\tau}} = \frac{\int_{-\infty}^{\infty} ab\eta^2 d\eta}{\int_{-\infty}^{\infty} ab\eta d\eta} = \frac{\int_{-\infty}^{\infty} ab(\alpha + Z\tau^{-1/3})^2 dZ}{\int_{-\infty}^{\infty} ab(\alpha + Z\tau^{-1/3}) dZ}.$$

To evaluate this a higher order expansion of the inner solutions is employed, as in [21], so that we have

$$a = \mathcal{A}^1\tau^{-1/3} + \mathcal{A}^2\tau^{-2/3} + \mathcal{A}^3\tau^{-1}$$

and

$$b = \mathcal{B}^1\tau^{-1/3} + \mathcal{B}^2\tau^{-2/3} + \mathcal{B}^3\tau^{-1}.$$

Then expanding  $r_f$  in large  $\tau$  yields

$$\frac{r_f}{2\sqrt{\tau}} \rightarrow \alpha + \frac{P_2}{P_1\tau^{1/3}} + \frac{P_3 + \alpha Q_3}{\alpha P_1\tau^{2/3}} - \frac{(P_2 + \alpha Q_2)P_2}{\alpha P_1^2\tau^{2/3}}$$

where  $P_1 = \langle \mathcal{A}^1\mathcal{B}^1 \rangle$ ,  $P_2 = \langle \mathcal{A}^1\mathcal{B}^1 Z \rangle$ ,  $P_3 = \langle \mathcal{A}^1\mathcal{B}^1 Z^2 \rangle$ ,  $Q_2 = \langle (\mathcal{A}^1\mathcal{B}^2 + \mathcal{A}^2\mathcal{B}^1) \rangle$  and  $Q_3 = \langle (\mathcal{A}^1\mathcal{B}^2 + \mathcal{A}^2\mathcal{B}^1 Z) \rangle$ , where  $\langle f, g \rangle = \int_{-\infty}^{\infty} fg dz$ .

Thus to first order we have

$$\frac{r_f}{2\sqrt{\tau}} \rightarrow \alpha + \frac{\langle \mathcal{A}^1\mathcal{B}^1 Z \rangle}{\langle \mathcal{A}^1\mathcal{B}^1 \rangle \tau^{1/3}}.$$

As this only involves the leading order solution we can express this in terms of the function  $G$  as

$$\frac{r_f}{2\sqrt{\tau}} \rightarrow \alpha + \frac{1}{(4\delta_b U\tau)^{1/3}} \frac{\int_{-\infty}^{\infty} G_{zz} z dz}{\int_{-\infty}^{\infty} G_{zz} dz}.$$

However, using the boundary conditions in system (37) we have  $\int_{-\infty}^{\infty} G_{zz} dz = [G_z]_{-\infty}^{\infty} = 1$  and  $\int_{-\infty}^{\infty} G_{zz} z dz = [G_z z - G]_{-\infty}^{\infty} = 0$ , so  $P_2 = 0$ . Thus,

$$\frac{r_f}{2\sqrt{\tau}} \rightarrow \alpha + O(\tau^{-2/3}) \quad (38)$$

and the first moment of the reaction rate corresponds to the point  $r_f = 2\alpha\sqrt{\tau} + O(\tau^{-1/6})$ , i.e. at the point where the large time asymptotic outer solutions satisfy  $a = b = 0$ .

Hence, just as in the case of planar reaction fronts, for the reaction  $A + B \rightarrow C$  the local maximum in the reaction rate and the first moment of the reaction rate coincide in the large time asymptotic limit, (at  $z = 0$  in the inner coordinate system).

#### B. Width of the reaction front

Now let's consider the second moment of the reaction rate

$$\frac{w_f^2 + r_f^2}{4\tau} = \frac{\int_0^{\infty} ab\eta^3 d\eta}{\int_0^{\infty} ab\eta d\eta} = \frac{\int_{-\infty}^{\infty} ab(\alpha + Z\tau^{-1/3})^3 dZ}{\int_{-\infty}^{\infty} ab(\alpha + Z\tau^{-1/3}) dZ}.$$

Then expanding  $r_f$  in large  $\tau$  yields

$$\begin{aligned} \frac{w_f^2 + r_f^2}{4\tau} &\rightarrow \\ &\alpha^2 + \frac{2\alpha P_2}{P_1\tau^{1/3}} + \frac{3P_3 + 2\alpha Q_3}{P_1\tau^{2/3}} - \frac{2(P_2 + \alpha Q_2)P_2}{\alpha P_1^2\tau^{2/3}}. \end{aligned}$$

Hence, using the result for  $r_f$ , we obtain

$$\frac{w_f^2}{4\tau} \rightarrow \frac{P_3}{P_1\tau^{2/3}} - \frac{P_2^2}{P_1^2\tau^{2/3}}.$$

Thus, using the results in the previous subsection that  $P_2 = 0$ , we obtain

$$w_f^2 \rightarrow 4\tau^{1/3} \frac{\langle \mathcal{A}^1 \mathcal{B}^1 Z^2 \rangle}{\langle \mathcal{A}^1 \mathcal{B}^1 \rangle}.$$

Again, as this only involves the leading order solution we can express this in terms of the function  $G$  as

$$w_f^2 \rightarrow \frac{(4\tau)^{1/3}}{(\delta_b U)^{2/3}} \frac{\int_{-\infty}^{\infty} G_{zz} z^2 dz}{\int_{-\infty}^{\infty} G_{zz} dz}$$

Hence, using the integral results we obtain

$$w_f \rightarrow \frac{2^{1/3} \sqrt{\Phi}}{(\delta_b U)^{1/3}} \tau^{1/6} \quad (39)$$

where  $\Phi = \int_{-\infty}^{\infty} G_{zz} z^2 dz$ . Numerically [31] found that  $\Phi \approx 1.90250$ .

We note that although the equation for  $w_f$  appears to be the same as what one obtains for a planar reaction front, see [31], the term  $U$  is different. In the large Pe limit, using  $\alpha = \sqrt{\text{Pe}} + \psi/\sqrt{2}$ , we find that

$$U \rightarrow \frac{2\sqrt{2}e^{-\psi^2}}{\sqrt{\pi}\text{erfc}(-\psi)}$$

which is  $\sqrt{2}$  times larger than the term  $U$  given in [31]. Thus in the large time asymptotic limit for large Pe, the concentration gradients around the radial reaction front are  $\sqrt{2}$  times larger those of a planar reaction front and the width of a radial reaction front is  $1/2^{1/6}$  of the width of a planar reaction front.

## VII. CONCLUSIONS

This article considers the analytical, numerical and small- and large-time asymptotic solutions of the reaction equation  $A + B \rightarrow C$  in a Hele-Shaw cell where a reactant solution  $A$  is injected as a point source into a reactant  $B$ . A polar-coordinate system is employed to accurately model the reaction line as it extends from the point source.

A Crank-Nicolson numerical method is employed to ascertain numerical solutions, showing that diffusion dominates over advection in the early stages of the slow flow regime. Advection is shown to dominate proceedings in the fast flow regime and no overall control is displayed in the moderate flow regime. In late stages of the experiment, the slow flow regime illustrates sharp concentration gradients near the centre of the sample, the moderate flow regime shows the maximum concentration of the product moving away from the centre of the sample

and the fast flow regime illustrates that the concentration gradients of all species tend to zero away from the reaction front, resembling the concentration profiles of the planar reaction problem.

Small- and large-time asymptotic solutions are found for a variety of special cases, each of which closely match the numerical solutions found using the finite-differences scheme. The effects of the parameters related to the Péclet number and the molecular diffusion coefficients are also investigated.

It would be of great interest if previous  $A+B \rightarrow C$  experiments in planar geometries could be reinvestigated in radial geometries and compared with the results found herein. For example, experiments using  $\text{Cu}^{2+}$  copper ions with disodium ethyl bis (5-tetrazolylazo) acetate trihydrate in [33, 34] or  $\text{Cu}^{2+}$  copper ions with calcium green in [35, 36], which use a variety of species concentrations and molecular diffusion coefficients, could be re-analysed to confirm the analysis within.

This theory could be applied in many experiments where the consumption of reagent can lead to unstable density distortions such as density fingering, which has not been considered here. For most liquids, viscosities vary very slowly with concentration changes, so in a dilute system it is usually valid to ignore viscosity variations and so viscous fingering instabilities can be neglected. Furthermore, in dilute systems buoyancy instabilities (usually 100 to 1000 times weaker in microgravity) will have no effect for small to intermediate times. The actual length of time the solution remains valid for is expected to strongly depend on the flow rates, diffusion coefficients, concentrations and the solutal expansion coefficients of the species. Nevertheless, the length of time for which the solutions are valid could be determined by performing a linear stability analysis on the spatially varying time dependent profiles to determine when the integral of the real part of the instantaneous growth of the instability becomes order 1, as this point the solutions are no longer valid. This remains a worthwhile exercise for the interested reader.

## Acknowledgements

PMJT would like to thank Damian Strier for fruitful discussions. The authors acknowledges Prodex (Belgium) for financial support.

## Appendix A: Lower limit of $\Gamma(a, x)$

Consider

$$G = \Gamma(\text{Pe}, y^2)$$

which by the definition of the incomplete Gamma function implies that

$$G_y = -2y^{2\text{Pe}-1}e^{-y^2}.$$

If  $Pe$  is very small, then there is a boundary layer near  $y = 0$ . Thus if we consider  $0 < y \ll 1$ , and expand the exponential term we obtain

$$G_y = -2y^{2Pe-1} + 2y^{2Pe+1} - \frac{y^{2Pe+3}}{2} + \dots$$

which can be directly integrated to yield

$$G = \Gamma(Pe) - \frac{y^{2Pe}}{Pe} + \frac{y^{2Pe+2}}{Pe+1} - \frac{y^{2Pe+4}}{4Pe+8} + \dots$$

where the integration constant is  $\Gamma(Pe)$  since the remaining terms in the expansion are all zero at  $y = 0$ . Hence,

$$\Gamma(Pe) - \Gamma(Pe, y^2) = \frac{y^{2Pe}}{Pe} - \frac{y^{2Pe+2}}{Pe+1} + \frac{y^{2Pe+4}}{4Pe+8} + \dots \quad (A1)$$

if both  $Pe$  and  $y$  are small. One notes that the term  $y^{2Pe}$  can be written as  $\exp(2Pe \ln(y)) \approx 1 + 2Pe \ln(y)$  as  $Pe$  is small.

In this study we shall also use the limit

$$\Gamma(x) \rightarrow \frac{1}{x} - \gamma + \left( \frac{\pi^2}{12} + \frac{\gamma^2}{2} \right) x + \dots \quad (A2)$$

as  $x$  tends to zero where  $\gamma$  is Euler's constant, which is approximately given by 0.5772156649.

#### Appendix B: Upper limit of $\Gamma(a, x)$

We recall that the solution to the equation

$$-2\eta a_\eta + (2Pe - 1) \frac{a_\eta}{\eta} = a_{\eta\eta}$$

is  $a = \Gamma(Pe, \eta^2)/\Gamma(Pe)$ . This function will be approximated by extending the expansion by Tan and Homsy [32]. We substitute  $\eta = \sqrt{Pe} + \xi/\sqrt{2}$  into the differential equation and expand in large  $Pe$  to obtain

$$\frac{a_{\xi\xi}}{a_\xi} = -2\xi + (\xi^2 - 1) \left[ \frac{1}{\sqrt{2Pe}} - \frac{\xi}{2Pe} + \dots \right]$$

This can be integrated to yield

$$a_\xi = c_1 \exp \left( -\xi^2 + \left[ \frac{\xi^3 - 3\xi}{3\sqrt{2Pe}} - \frac{\xi^4 - 2\xi^2}{8Pe} + \dots \right] \right).$$

Then expanding in large  $Pe$  yields

$$a_\xi = c_1 e^{-\xi^2} \left[ 1 + \frac{\xi^3 - 3\xi}{3\sqrt{2Pe}} + \frac{36\xi^2 - 21\xi^4 + 2\xi^6}{72Pe} + \dots \right]$$

By integrating this and using the boundary conditions that  $a$  tends to 1 as  $\xi$  tends to  $-\infty$  and  $a$  tends to zero as  $\xi$  tends to  $\infty$ , we obtain the approximate solution

$$a = \frac{\text{erfc}(\xi)}{2} + \frac{e^{-\xi^2}}{6\sqrt{\pi}} \left[ \frac{\xi^2 - 2}{\sqrt{2Pe}} + \frac{6\xi - 8\xi^3 + \xi^5}{12Pe} + \dots \right] \quad (B1)$$

as  $Pe$  tends to infinity. Numerically, one finds that the second order expansion shown in equation (B1), along with a first order expansion and a zeroth order expansion have errors of approximately  $0.0086/Pe^{3/2}$ ,  $0.0128/Pe$  and  $0.133/\sqrt{Pe}$ , respectively, as  $Pe$  tends to infinity.

As an aside, one notes that a slight improvement to the zeroth order approximation is

$$a = \frac{1}{2} \text{erfc} \left( \xi + \frac{1}{3\sqrt{2Pe}} \right)$$

which has an error approximately given by  $0.025/\sqrt{Pe}$ .

In this study we shall also use the limit

$$\Gamma(x) \rightarrow \sqrt{2\pi} e^{-x} x^{x-\frac{1}{2}} \left( 1 + \frac{1}{12x} + \dots \right) \quad (B2)$$

as  $x$  tends to infinity, from equation (6.1.37) from Abramowitz and Stegun [29].

#### Appendix C: Comparing planar and radial reaction fronts for fast flows

Let us next consider the transport equations (7) for a radial reaction front in a coordinate system moving with the contact line  $\xi = \sqrt{2}(\eta - \sqrt{Pe})$ . The transport equations become

$$\begin{aligned} \tau a_\tau - (\sqrt{2Pe} + \xi) \frac{a_\xi}{2} + \frac{(2Pe - 1)a_\xi}{2(\sqrt{2Pe} + \xi)} &= \frac{a_{\xi\xi}}{2} - ab\tau \\ \tau b_\tau - (\sqrt{2Pe} + \xi) \frac{b_\xi}{2} + \frac{(2Pe - 1/\delta_b)b_\xi}{2(\sqrt{2Pe} + \xi)} &= \frac{b_{\xi\xi}}{2\delta_b} - ab\tau \\ \tau c_\tau - (\sqrt{2Pe} + \xi) \frac{c_\xi}{2} + \frac{(2Pe - 1/\delta_c)c_\xi}{2(\sqrt{2Pe} + \xi)} &= \frac{c_{\xi\xi}}{2\delta_c} + ab\tau. \end{aligned}$$

For fast flow rates we expand this system in large  $Pe$  to obtain

$$\begin{aligned} \tau a_\tau - \xi a_\xi &= \frac{a_{\xi\xi}}{2} - ab\tau \\ \tau b_\tau - \xi b_\xi &= \frac{b_{\xi\xi}}{2\delta_b} - ab\tau \\ \tau c_\tau - \xi c_\xi &= \frac{c_{\xi\xi}}{2\delta_c} + ab\tau \end{aligned}$$

where corrections of the order  $O(Pe^{-1/2})$  have been neglected. If we then seek a similarity solution, so that the solution becomes independent of  $\tau$ , then one obtains

$$-\xi a_\xi = \frac{a_{\xi\xi}}{2}, \quad -\xi b_\xi = \frac{b_{\xi\xi}}{2\delta_b}, \quad -\xi c_\xi = \frac{c_{\xi\xi}}{2\delta_c}.$$

which is identical to the system of similarity equations that one obtains for a planar reaction front.

Hence, in the large Péclet number limit, in a reference frame moving with the injected fluid, the radial reaction front behaves just like the planar reaction front when a similarity solution exists. Such solutions exist in both

the small and large time asymptotic limit, and hence as  $Pe$  tends to infinity, we find that

$$r_m = r_c + x_m/\sqrt{2}, \quad r_f = r_c + x_f/\sqrt{2} \quad (C1)$$

where  $r_m$  is the location where the reaction rate is maximum and  $r_f$  is the first moment of the reaction rate for a

radial reaction front and  $x_m$  and  $x_f$  are the corresponding quantities for a planar reaction front. Thus the distance between the radial reaction front and the contact line is equal to the distance that a planar reaction front travels divided by  $\sqrt{2}$ .

- 
- [1] S. A. Rice, *Diffusion-Limited Reactions* (1st edition), Elsevier Science (1985).
  - [2] D. ben-Avraham and S. Havlin, *Diffusion and Reactions in Fractals and Disordered Systems* (2000)
  - [3] A. Zalts, C. El Hasi, D. Rubio, A. Urena and A. D'Onofrio, Phys. Rev. E **77**, 015304(R) (2008).
  - [4] C. Almarcha, P. M. J. Trevelyan, P. Grosfils and A. De Wit, Phys. Rev. Lett. **104**, 044501 (2010).
  - [5] C. Almarcha, P. M. J. Trevelyan, L. Riolfo, A. Zalts, C. El Hasi, A. D'Onofrio and A. De Wit, J. Phys. Chem. Lett. **1**, 752 (2010).
  - [6] C. Almarcha, Y. R'Honi, Y. De Decker, P. M. J. Trevelyan, K. Eckert and A. De Wit, J. Phys. Chem. B **115**, 9739 (2011).
  - [7] Y. Shi and K. Eckert, Chem. Eng. Sci. **61**, 5523 (2006)
  - [8] A. Riaz, M. Hesse, H. A. Tchelepi and F.M. Orr, Jr, J. Fluid Mech. **648**, 87 (2006)
  - [9] K. Eckert, M. Acker and Y. Shi, Phys. Fluids **16**, 385 (2004).
  - [10] D. A. Bratsun, Y. Shi, K. Eckert and A. De Wit, Europhys. Lett. **69**, 746 (2005).
  - [11] L. Rongy, P. M. J. Trevelyan and A. De Wit, Phys. Rev. Lett. **101**, 084503 (2008).
  - [12] G. Venzl, J. Chem. Phys. **85**, 2006 (1986).
  - [13] L. Gálfi and Z. Rácz, Phys. Rev. A **38**, 3151 (1988).
  - [14] Y. -E. L. Koo and R. Kopelman, J. Stat. Phys. **65**, 893 (1991).
  - [15] A. Yen and R. Kopelman, Phys. Rev. E. **56**, 3694 (1997).
  - [16] Z. Koza, J. Stat. Phys. **85**, 179 (1996).
  - [17] M. Sinder and J. Pelleg, Phys. Rev. E **62**, 3340 (2000).
  - [18] S. Cornell, M. Droz and B. Chopard, Phys. Rev. A **44**, 4826, (1991).
  - [19] S. Cornell and M. Droz, Phys. Rev. Lett. **70**, 3824 (1993).
  - [20] S. Cornell, Z. Koza and M. Droz, Phys. Rev. E **52**, 3500, (1995).
  - [21] P. M. J. Trevelyan, Phys. Rev. E **79**, 016105 (2009).
  - [22] P. M. J. Trevelyan, Phys. Rev. E **80**, 046118 (2009).
  - [23] H. Taitelbaum, S. Havlin, J. E. Kiefer, B. Trus and G. H. Weiss, J. Stat. Phys. **65**, 873, (1991).
  - [24] H. Taitelbaum, Y.- E. L. Koo, S. Havlin, R. Kopelman and G.H. Weiss, Phys. Rev. A **46**, 2151 (1992).
  - [25] I. Hecht and H. Taitelbaum, Phys. Rev. E **74**, 012101 (2006).
  - [26] H. Taitelbaum and Z. Koza, Physica A **285**, 166 (2000).
  - [27] F. Brau, G. Schuszter and A. De Wit, Phys. Rev. Lett. **118**, 134101 (2017).
  - [28] G. Schuszter, F. Brau and A. De Wit, Environ. Sci. Technol. Lett. **3**, 156-159 (2016).
  - [29] M. Abramowitz and I. A. Stegun, *Handbook of Mathematical Functions*, Dover, New York, 1972.
  - [30] E. T. Whittaker and G. N. Watson, *A Course of Modern Analysis*, Cambridge University Press, Cambridge, 1927.
  - [31] P. M. J. Trevelyan, D. E. Strier, A. De Wit, Phys. Rev. E **78**, 026122 (2008).
  - [32] C. T. Tan and G. M. Homsy, Phys. Fluids **30**, 1239 (1987).
  - [33] Y.- E. L. Koo and R. Kopelman, J. Stat. Phys. **65**, 893-918 (1991)
  - [34] S. H. Park, S. Parus, R. Kopelman and H. Taitelbaum, Phys. Rev. E **64**, 055102(R) (2001)
  - [35] C. N. Baroud, F. Okkels, L. Ménétrier and P. Tabeling, Phys. Rev. E **67**, 060104(R) (2003)
  - [36] S. H. Park, H. Peng, R. Kopelman and H. Taitelbaum, Phys. Rev. E **75**, 026107 (2007)